

Fine-grained domain counting and percolation analysis in 2D lattice systems with linked-lists

Hrushikesh Sable,^{1,2} Deepak Gaur,^{1,2} and D. Angom^{1,3}

¹*Physical Research Laboratory, Ahmedabad - 380009, Gujarat, India*

²*Indian Institute of Technology Gandhinagar, Palaj, Gandhinagar - 382355, Gujarat, India*

³*Department of Physics, Manipur University, Canchipur - 795003, Manipur, India*

(Dated: January 3, 2022)

We present a fine-grained approach to identify clusters and perform percolation analysis in a 2D lattice system. In our approach, we develop an algorithm based on the linked-list data structure and the members of a cluster are nodes of a path. This path is mapped to a linked-list. This approach facilitates unique cluster labeling in a lattice with a single scan. We use the algorithm to determine the critical exponent in the quench dynamics from Mott Insulator to superfluid phase of bosons in 2D square optical lattices. The result obtained are consistent with the Kibble-Zurek mechanism. We also employ the algorithm to compute correlation lengths using definitions based on percolation theory. And, use it to identify the quantum critical point of the Bose Glass to superfluid transition in the disordered 2D square optical lattices. In addition, we also compute the critical exponent of the transition.

I. INTRODUCTION

There are strong motivations across research disciplines to develop novel approaches and computational methods to study the percolation theory. The percolation theory provides a simple and unifying framework to understand clustering of particles in a medium. It has wide applications like the permeation of fluid in porous media [1], spontaneous magnetization of dilute ferromagnets [2], polymer gels [3] to mention a few. The study of the clustering or connectivity of the particles gains importance as it determines the macroscopic properties of the system. For example, the electrical conduction through a composite mixture of conducting and insulating materials is described by the percolation analysis of the conducting material in the mixture.

A generic percolation problem consists of an infinite lattice populated with two classes of lattice sites at random. These are denoted as occupied and unoccupied sites [4, 5]. A group of occupied sites connected through bonds forms a cluster. The probability of a site being occupied determines the distribution and size of the clusters. The system undergoes a percolation phase transition, when the probability exceeds a critical value. Then, there exists a spanning cluster which extends from one edge of the system to the opposite edge. Although the percolation problem as stated is straightforward, analytical approaches are limited. It is, however, possible to gain an understanding of the system using numerical methods. A prominent algorithm used in percolation analysis is the Hoshen-Kopelman (HK) cluster multiple labeling algorithm [6]. The application of the percolation analysis and of the HK algorithm are in diverse fields like - food and chemical engineering [7, 8], ecology [9] and biology [10]. The basic essence of the algorithm is to scan through the lattice and identify the occupied sites. During the scan, the occupancy of neighbouring sites are also checked and the connected occupied sites are assigned a cluster label. The key point of the algorithm is that the neighbouring sites are allowed to have different labels, but with a record that they belong to the same cluster. There are now several variations of the HK [11–15] including a proposal to use linked-list to group the clusters belonging to the same domain [16].

In this work, we present a fine-grained algorithm of cluster labeling and describe its application in the percolation analysis of 2D lattices. The algorithm employs the linked list data structure. Using which we can define a path connecting all the sites belonging to a cluster. This facilitates the scanning of the lattice in a single scan. Since the path links sites, it is fine-grained and we can employ it to analyse cluster properties. That include determination of boundaries, easy identification of spanning cluster, and calculation of various cluster properties like center of mass, radius of gyration, correlation length, etc. Our approach is well suited for detailed analysis of results encountered in the studies of optical lattices where we obtain a set of configurations and wish to examine it using the tools from percolation theory. However, it must be emphasized that to simulate percolation the Newman-Ziff algorithm [17] is the method of choice.

We address two important problems in the physics of ultracold bosonic atoms in optical lattices using the algorithm. First, we study the quantum quench dynamics of bosons in the optical lattices from the Mott Insulator (MI) to the superfluid (SF) phase. Using our method we identify the clusters or domains and show that the number of domains follows a power-law dependence on the quench rate. This is consistent with the Kibble-Zurek mechanism (KZM) [18–22]. It is to be mentioned that recent works on ultracold atoms have reported similar results in quantum quenches across different quantum phases [23–26]. Further, as to be expected, we show that the dependence of the defect density on the quench rate has the same power-law exponent as the number of domains. And, second, we study the critical properties in the Bose glass (BG) to SF transition of bosons in disordered optical lattices. The BG phase is insulating yet compressible and it is characterized by the SF *puddles* with an MI background [27–30]. Using our method we compute the geometrical properties of the SF clusters. As mentioned, our fine-grained method stores locations of all the sites of a cluster. From this information, we calculate the percolation correlation length of the system across the BG-to-SF transition. As expected, the correlation length peaks at the transition point, and has power-law dependence on the reduced hopping strength. The critical exponent ν which quantifies the power-law reveals that the BG-to-SF transition belongs to the random site percolation universality

class of 2D lattices.

The remainder of this article is organized as follows. We first introduce linked-lists and discuss mapping of the domains to a linked-list in Section II. We then discuss the algorithm of our method in the Section III. We describe the identification of the boundary of the cluster in Section IV. In Section V, we discuss the application of our method to the MI-SF quench dynamics. Then, in the Section VI, we present the study of the BG-to-SF transition from the perspective of percolation theory. We summarize our main results and present discussions in Section VII.

II. MAPPING DOMAIN TO A LINKED-LIST

For a better description of our method we consider a 2D square lattice and each of the lattice sites are labeled at random with either 0 or -1 . As mentioned earlier, the task at hand is to identify and enumerate the domains with either of the two labels. For illustration let us take the domains of sites with the label 0. The lattice sites are denoted by (i, j) , where i is the

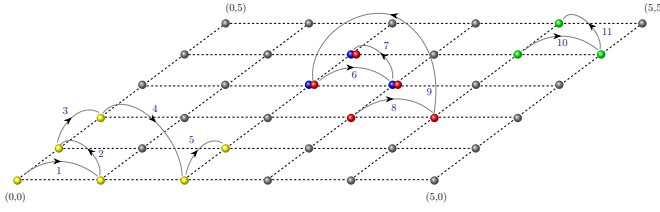


FIG. 1. A schematic diagram to illustrate the paths defining a cluster. The arrows indicate the links between sites constituting a domain. The gray shaded lattice sites are labeled -1 . Here distinct domains are identified with different colors which are representative of domain labels. During the scan, different parts of a same domain may get identified with different labels. However, they should be identified as a single domain. In the figure, the red and blue colored sites denotes such a possibility.

column index and j is the row index. These correspond to the x - and y -axis coordinates, respectively, in the xy -plane. The central idea of our approach is to use the concept of linked-list data structure [31] to describe a domain. A linked-list stores a data sequence in non-contiguous memory locations. And, in a linked-list, each element of the sequence is stored in a node of the list and each node has a reference or a link to the memory location of the next element in the sequence. This continues till the last element of the sequence. The advantage of using linked-list is the ease of updating it to insert a new node or merging multiple linked-lists. In the present work, to define a domain each lattice site of the system is uniquely mapped to the node of a unidirectional linked-list. The node is, then, linked to another lattice site which belongs to the same domain. This way each domain is represented by one linked-list. Thus, once we know the starting node of a linked-list we can traverse through all the lattice sites belonging to a domain. For this reason, the linked-list associated with a domain can also be thought of as a *path* traversing through it.

Here after, we use path to refer to the linked-list. Such a path passes through each lattice site in the domain once. Our main objective is, then, to enumerate the number of such distinct paths corresponding to the domains of lattice sites with the label 0. Then, the number of such paths is the number of domains.

To define the link in the node corresponding to the (i, j) lattice site, we introduce two variables $x_{i,j}$ and $y_{i,j}$. The variable $x_{i,j}$ ($y_{i,j}$) is the location along the x (y) direction of the next lattice site in the path. These variables should have well defined values for the lattice sites at the beginning and intermediate nodes of a path. But, this is not required for the last node of a path. To distinguish the end node we assign negative integers to these two variables for this node. Since we use unidirectional linked-list it is essential to define the location of the first lattice site in a path or the first node of the path. For this we introduce two variables for each path α^k and β^k , these are the x and y locations of the first lattice site of the k th path, respectively. To facilitate further analysis of the domains, we denote the total number of nodes or lattices sites in the k th domain by \mathcal{N}^k . And, introduce γ^k and δ^k as the pair of variables which define the x and y lattice site corresponding to the last node of the path. Suppose $\{x_{i,j}^k, y_{i,j}^k\}$ is the set of the links of the k th path, then the set of variables

$$\{\alpha^k, \beta^k, x_{i,j}^k, y_{i,j}^k, \gamma^k, \delta^k, \mathcal{N}^k\}, \quad (1)$$

defines the k th path or the domain uniquely. The schematic diagram of typical paths defining clusters on a 2D square lattice are shown in Fig. 1.

III. DOMAIN IDENTIFICATION

To identify the domains, we check the label at each lattice site column wise. We start the scan from the left edge. That is, the column scanning is done left to right or in the increasing order of the lattice site index along the x direction. During the scan, we check the label at a lattice site, say (i, j) . If the label of the site is 0, then, it is relabelled as k . This identifies the lattice site as a member of the k th domain and the site is linked to the path. This number, following earlier description, is also the sequence number of the domain. There is no change in the label if the lattice site is already identified as the member of a domain. Then, we scan the label of the right nearest neighbour lattice site $(i + 1, j)$. If the label of this site is also 0, then, it is relabelled as k . This identifies the lattice site $(i + 1, j)$ as a member of the same domain. Accordingly, we update the path to include the site. Then, the scan is continued to the lattice site $(i, j + 1)$, the nearest neighbour above (i, j) . In case the label of the lattice site (i, j) is -1 , then the scan proceeds to $(i, j + 1)$. That is, the label of the right nearest neighbour is not checked. This process is repeated till the topmost lattice site of the column is reached. Then, we move to the next column and continue this process till the entire system is covered. Two distinct cases arise. First, the left edge column, the column scanned first. Since, this is the starting column, domains are yet to be identified. And, second, the remaining columns. These are the columns in the bulk and the right edge

column. To record the number of domains identified we use the variable κ .

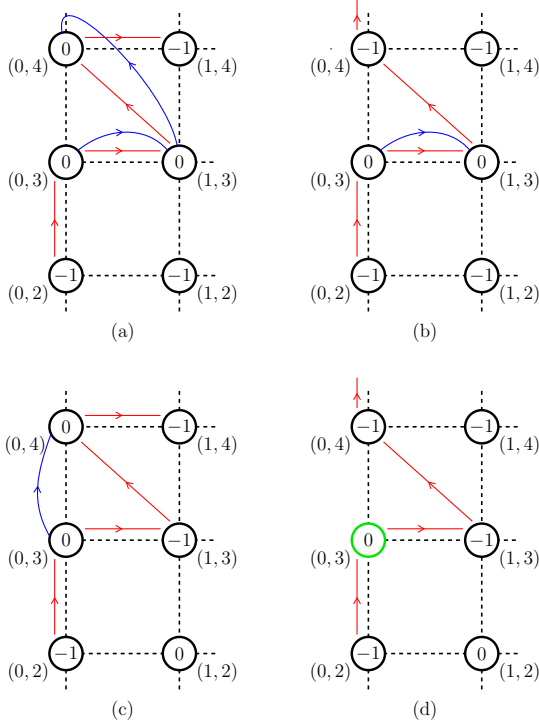


FIG. 2. Schematic illustration of the possibilities arising in the scan along the lattice sites of the left edge column. The red arrows indicate the scanning direction, and the blue arrows represent the inter-site links. The sites are represented by circles and the labels are shown within the circles. Panels (a)-(c) represent different cases of linking the site (0, 3) with its right and/or upper neighbours. And panel (d) represents the possibility of an isolated site as a domain.

A. Left edge column

At the beginning of the scan, we initialize the variable κ to zero. And, it is incremented by one when a new domain is encountered. For example, assume that the lattice site (0, 3) is the first lattice site along the column which has label 0. During the scan, on reaching this lattice site, we increment κ to 1 and relabel the lattice site (0, 3) as 1. This is a newly identified domain, hence, it is the first node of the path for the domain with $k = 1$ as well as the last. Accordingly, set the first node variables $\alpha^1 = 0$ and $\beta^1 = 3$. And, the last node variables $\gamma^1 = 0$ and $\delta^1 = 3$. In addition, the counter for the number of the nodes in the domain is updated as $\mathcal{N}^1 = 1$. Since this is the last node of a path we set $x_{0,3}^1 = -2$ and $y_{0,3}^1 = -2$. The choice of -2 is arbitrary. It is a number which is not assigned to any of the variables. Then, we check the label of the right nearest neighbour lattice site (1, 3). There are four possible outcomes.

Case A: If this lattice site has 0 label, then it is relabelled as 1. And, shift the end node of the path to (1, 3) by assigning

$x_{1,3}^1 = x_{0,3}^1$ and $y_{1,3}^1 = y_{0,3}^1$. Accordingly, update the last node variables to $\gamma^1 = 1$ and $\delta^1 = 3$. The path is, then, updated by linking the lattice site (0, 3) to (1, 3) by setting $x_{0,3}^1 = 1$ and $y_{0,3}^1 = 3$. Then, we continue the scan along the column to the lattice site (0, 4) located above (0, 3). If this too is 0, we extend the path to this lattice site by making this the end node with the assignment $x_{0,4}^1 = x_{1,3}^1$ and $y_{0,4}^1 = y_{1,3}^1$, and update the end node variables to $\gamma^1 = 0$ and $\delta^1 = 4$. Then, connect it to the lattice site (1, 3) by redefining $x_{1,3}^1 = 0$ and $y_{1,3}^1 = 4$. This possibility is schematically shown in Fig.2(a).

Case B: The lattice site (1, 3) is labelled zero but not (0, 4). This possibility is depicted schematically in Fig.2(b). Then, the last step of variable assignments in Case A is not required.

Case C: The lattice site (1, 3) is labelled -1 , but (0, 4) is labelled 0. This is similar to the Case A, but without the intermediate step of linking the lattice site (1, 3). The situation is schematically shown in Fig.2(c).

Case D: This is the last case and correspond the situation when both the lattice sites (1, 3) and (0, 4) are -1 . Then, the (0, 3) is an isolated domain as shown in Fig.2(d).

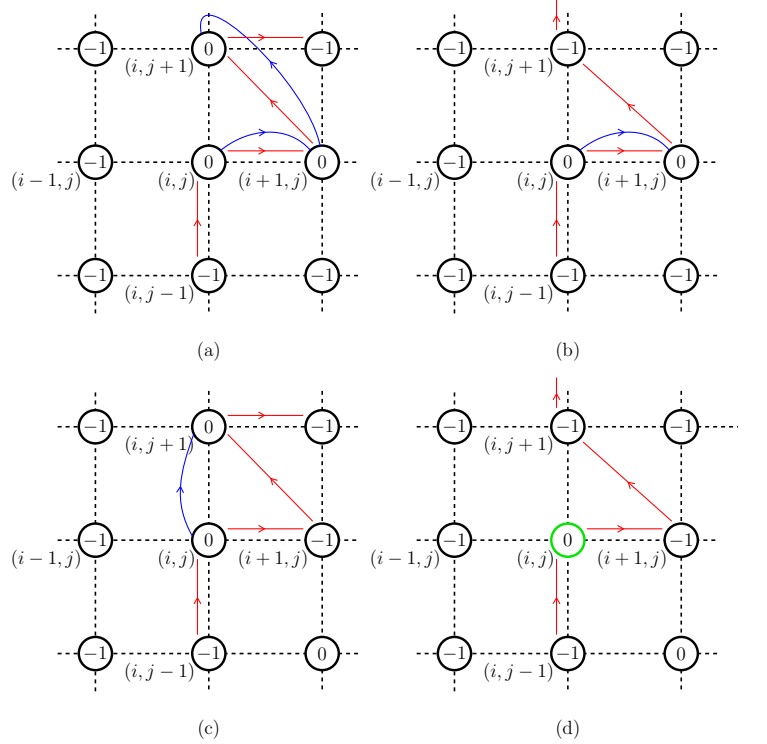


FIG. 3. Schematic illustration of the case of the new domain formation for the lattice sites in the bulk. The red arrows indicate the scanning direction, and the blue arrows represent the inter-site links. The steps of scanning and linking the nodes in the path are similar to the one denoted in Fig. 2

B. Column in the bulk and right edge

The general steps of scanning the remaining columns of the systems is the same. For illustration, as a general case, let us consider the scanning of the i th column and assume that we have reached the j th row in the column. That is, the lattice site to be scanned is (i, j) . If the label of the lattice site is -1 , this is a trivial case and the site does not belong to any domain. The scan can continue to the next lattices site $(i, j + 1)$ in the column. In case the label of the lattice site (i, j) is not -1 , then, there are three possible outcomes of the scan.

1. New domain

Consider the label of the lattice site (i, j) is 0, then the current value of κ is incremented by one. The new value of κ is taken as the value of k , and the lattice site (i, j) is relabelled with this value. Like in the case of the left edge, set $x_{i,j}^k = -2$ and $y_{i,j}^k = -2$ for the path and $\mathcal{N}^k = 1$ for the number of members. And, then, set the first (last) node variables of the path as $\alpha^k = i$ ($\gamma^k = i$) and $\beta^k = j$ ($\delta^k = j$). We, then, scan the lattice site $(i + 1, j)$, and followed by $(i, j + 1)$. Similar to the case of the left edge column, discussed earlier, we can have four possible outcomes. The only difference is, in each of the cases the lattice site $(0, 3)$ is replaced by (i, j) . The four cases are schematically shown in Fig.3.

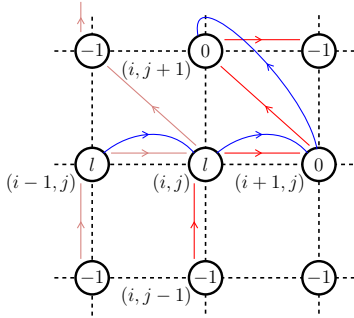


FIG. 4. Schematic illustration of a case when the lattice site being scanned is in an old domain. As shown, the site (i, j) is labeled with label l . In this case, the right and upper neighbours are checked for label 0, and are added to the path.

2. Old domain

Consider the label of the lattice site is a positive integer l , indicating that (i, j) is already identified as a member of the l th domain. In this case, no modification of the variables of the lattice site are required. We, then, check the label of the right nearest neighbour lattice site $(i + 1, j)$. If the label is -1 , then the scan continues to the upper nearest neighbour lattice site $(i, j + 1)$. On the other hand, if the label is 0, then the lattice site belongs to the l th domain. So, we have to update

the domain and path variables to include $(i + 1, j)$ as a part of this domain. For this, we change the label of $(i + 1, j)$ to l and link the end node of the l th path to the $(i + 1, j)$ by setting $x_{\gamma^l, \delta^l}^l = i + 1$ and $y_{\gamma^l, \delta^l}^l = j$. Then, $(i + 1, j)$ is made the end node by assigning $x_{i+1,j}^l = -2$ and $y_{i+1,j}^l = -2$, and then, update the end node variables to $\gamma^l = i + 1$ and $\delta^l = j$. The modifications associated with the addition of a node is complete by incrementing the node count \mathcal{N}^l by one. And, the schematic diagram of this possibility is shown in the Fig.4. For illustration, the path identified in the previous column scanning is shown in light red. In general, except for the label l of site (i, j) , the three cases—A, B and C—discussed earlier are applicable in the present case as well. The Case D is not applicable, as it corresponds to a domain of isolated site. Like the earlier cases, the next step is to consider the possibility of linking the upper neighbour lattice site $(i, j + 1)$. It is to be noted that the four cases shown in the Fig. 3 and the case of the old domain discussed covers the possibilities encountered during the scanning of the sites.

Based on the discussions, in general, appending of a site (i, j) as a new node to a path consists of three steps. First, the site (i, j) is linked to the current end node of the path. Second, the site (i, j) is identified as the end node. And, third, the addition of the node is completed with by updating the end node variables and node count variable. These steps are common to all the cases.

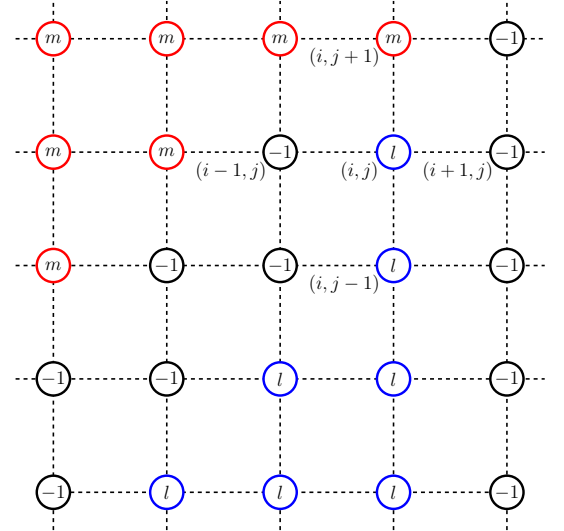


FIG. 5. Schematic illustration of a possibility of the domain merging case. As shown in the figure, distinct labels l and m occur on the neighbouring sites (i, j) and $(i, j + 1)$ respectively. So these two domains are merged.

3. Domain merging

Merging of two domains occurs when the labels of the neighbouring lattice sites along the column (i, j) and $(i, j + 1)$ are positive integers but different. As an example, consider

the labels of these sites are l and m , respectively and assume $l < m$. A representative case of such a situation is shown in Fig.5. Following the conventions adopted, the domain variables of the two are $\{\alpha^l, \beta^l, x_{i,j}^l, y_{i,j}^l, \gamma^l, \delta^l, \mathcal{N}^l\}$ and $\{\alpha^m, \beta^m, x_{i,j}^m, y_{i,j}^m, \gamma^m, \delta^m, \mathcal{N}^m\}$. To merge the two domains, the first step is to link the two corresponding paths and consolidate the two into a single one. For this the last node of the l th domain is linked to the first node of the m th domain. And, it is done by setting $x_{\gamma^l, \delta^l}^l = \alpha^m$ and $y_{\gamma^l, \delta^l}^l = \beta^m$. As a convention, we tag the merged domain with the variables corresponding to the one with the lower label value, in this case l . The merger is complete by updating the last node variables as $\gamma^l = \gamma^m$ and $\delta^l = \delta^m$, and the total number of lattice sites in the domain $\mathcal{N}^l = \mathcal{N}^l + \mathcal{N}^m$. As a last step, the m th domain is effectively nullified by setting $\mathcal{N}^m = 0$.

IV. CHARTING THE BOUNDARY

After we identify the domains, the next step is to map their boundaries. The boundary here means the outer edge of the domain. It defines the geometry of the domain. It excludes the internal boundaries associated with voids within the domains. Determining the boundary is essential to investigate the properties of the domains and apply the methods rooted in the percolation theory. To identify the boundary we *march* along it in the clock-wise direction, one bond at a time. For a domain, the starting site of the march (x_s, y_s) is identified as the left most site along one of the rows. Then the march is initiated after identifying the hop along the boundary to reach (x_s, y_s) . We refer to this as the *prior hop*.

A. Identifying the prior hop

The starting point (x_s, y_s) , as mentioned earlier, is the left most site of the domain of label m along a row. Hence, there are only two possibilities of the prior hop through which it can reach the site. These are as shown in the Fig.6(a) and (b). Thus, it is sufficient to check the label at the two lattice sites (x_{s-1}, y_s) and (x_s, y_{s-1}) . The one with label m defines the originating site of the prior hop. With this information we can initiate the march. At the later hops too, the determination of the next hop requires the identification of the previous hop and this information is at hand once the march begins.

B. Clockwise scan

After the identification of the prior hop, we scan the other three nearest neighbours of the site (x_s, y_s) to identify the next site on the boundary. The scanning is done in the clock-wise direction, with respect to the orientation of the prior hop. This is schematically shown in Fig.6(c) and (d). And, the scan is terminated when we encounter a neighbour with label m . Let this neighbour be identified as $(x_{s'}, y_{s'})$ and it is the next site on the boundary. If all the three neighbours have label -1 , then the march proceeds by retracing along the prior

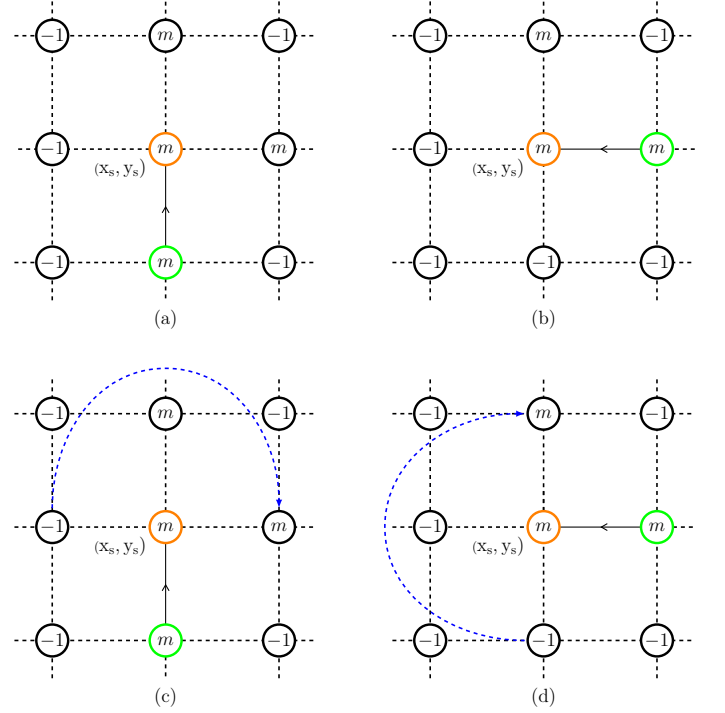


FIG. 6. Schematic illustration for the boundary *march*. The march is started from the site (x_s, y_s) , highlighted by the peach color. The black arrow represents the prior hop to reach the site (x_s, y_s) . As illustrated in text, this can be either a upward prior hop (case (a)) or leftward prior hop (case (b)). In (c) and (d), the blue dashed arrow indicates the clockwise scanning of the neighbours of (x_s, y_s) with respect to the orientation of the prior hop.

hop and origin of the prior hop is identified as the lattice site (x'_s, y'_s) . The bond connecting the two lattice sites (x_s, y_s) and (x'_s, y'_s) defines the orientation of the prior hop to scan for the next lattice site on the boundary after (x'_s, y'_s) . This process of scanning is repeated till we return to the starting site (x_s, y_s) .

As a representative case, we show the path along the boundary of a cluster in Fig.7. The starting site (x_s, y_s) is the left most site of the bottom row, and is highlighted in green color. The prior hop to reach (x_s, y_s) is leftward in this case, and shown by a gray arrow. Once the starting site and the prior hop are identified, the scanning of nearest neighbours proceeds to identify the next site on the boundary. As explained, the march is completed when we return to the initial starting site (x_s, y_s) . An important prerequisite for the boundary march is thus the identification of the starting site and the prior hop.

V. MI-SF QUENCH DYNAMICS

The MI phase to the SF phase quench dynamics of the Bose-Hubbard model [27], a model which describes the physics of ultracold bosons in optical lattices [32], has been experimentally realized [33]. During the quench, as the sys-

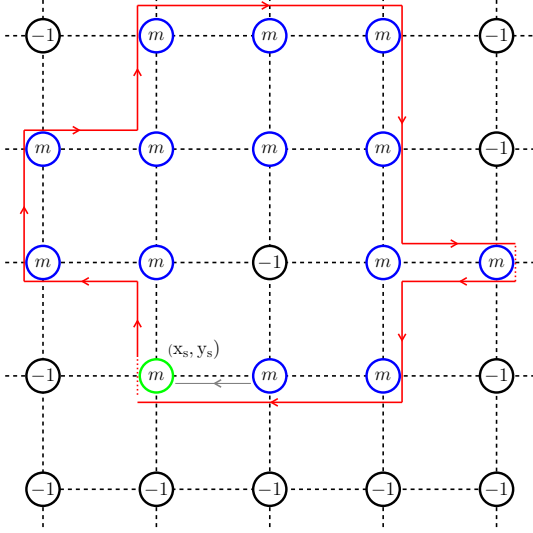


FIG. 7. Schematic illustration of the march along the boundary of a cluster. The site (x_s, y_s) shown in green color is the starting site of the march. The prior hop to reach the site (x_s, y_s) is shown by the gray colored arrow. The red arrows denote the directionality of the boundary march of the cluster shown in the figure.

tem crosses the critical point, SF domains are formed within MI as a background. We quantify the number of the SF domains using our domain counting algorithm. To discuss the dynamics, we first introduce the BHM Hamiltonian.

A. BHM Hamiltonian

The BHM Hamiltonian which describes the physics of ultracold bosonic atoms loaded in a 2D square optical lattice is [27, 32]

$$\hat{H} = - \sum_{\langle i,j \rangle} J \left(\hat{b}_i^\dagger \hat{b}_j + \text{H.c.} \right) + \sum_i \hat{n}_i \left[\frac{U}{2} (\hat{n}_i - 1) - \mu \right], \quad (2)$$

where $i \equiv (p, q)$ represent the lattice indexes, and $j \equiv (p', q')$ are the indexes of its neighbouring lattice site, \hat{b}_i^\dagger (\hat{b}_i) are the creation (annihilation) operators, \hat{n}_i is the bosonic occupation number operator and the summation indexes within $\langle \dots \rangle$ denote the sum over the nearest neighbours. Further, J is the hopping strength, $U > 0$ is the on-site inter-atomic interaction strength, and μ is the chemical potential.

The incompressible MI state and the compressible SF state are the two ground states of the BHM Hamiltonian in the strongly interacting ($J/U \ll 1$) and weakly interacting ($J/U \gg 1$) domains, respectively [27, 32]. The quantum phase transition between these two phases has been observed experimentally [34, 35]. The MI state has integer commensurate lattice site occupancies, and the bosons are pinned to the lattice sites. The SF state, on the other hand, features a real valued occupancy, and it is a conducting phase. The two

phases are identified base on the SF order parameter

$$\phi_{p,q} = \langle \hat{b}_{p,q} \rangle. \quad (3)$$

It is zero in the MI phase and non-zero in the SF phase. For a homogeneous lattice system, $\phi_{p,q}$ is uniform throughout the lattice. For our studies, we use the Single site Gutzwiller mean-field (SGMF) method to obtain the ground state of the model. In this method, the annihilation (creation) operators in Eq.(2) are separated into a mean-field ϕ (ϕ^*) and a fluctuation operator [36, 37]. The Hamiltonian in Eq.(2) can then be approximated as the mean-field Hamiltonian which is a sum of single site Hamiltonians $\hat{H}_{\text{MF}} = \sum_{p,q} \hat{h}_{p,q}$. We perform self-consistent calculation of $\phi_{p,q}$ till the desired convergence is obtained. The details of using this method in our computations are given in our previous works [30, 38–43].

B. Quench dynamics

To study the MI-SF quench dynamics of the system, the hopping amplitude J is ramped from an initial value J_i to a final value J_f . These are chosen such that J_i and J_f correspond to the MI and SF phases, respectively. The remaining parameters of the system are held fixed. Then, the temporal evolution of the system during the quench and afterwards is described by the time-dependent Schrödinger equation

$$i\hbar \partial_t |\psi\rangle_{p,q} = \hat{h}_{p,q} |\psi\rangle_{p,q}, \quad (4)$$

where $|\psi\rangle_{p,q}$ is the wavefunction at site (p, q) . Due to the intersite coupling through the order parameter ϕ , we obtain a set of coupled partial differential equations. These are solved using the fourth order Runge-Kutta method. To start the quench, we obtain the equilibrium wavefunction with the $J = J_i$, and introduce phase and density fluctuations to it [43]. These fluctuations simulate the quantum fluctuations essential to drive the quantum phase transition. To calculate system properties we take the ensemble average of a set consisting of 80 such randomized initial states.

We examine the non-equilibrium dynamics of the system during the quench from the KZM perspective. It categorizes the quench dynamics into three temporal regimes [44, 45], corresponding to the adiabatic, impulse and adiabatic regime. These temporal regimes arise due to the critical slowing down near the quantum critical point (QCP). It predicts the rate of the topological defects formation during the course of the quench dynamics [18–22]. These defects are generated at the meeting points of the domains of the symmetry broken SF phase. And, this is due to the local gauge choices of the order parameter associated with the domains. It is to be mentioned that the transition from MI to SF phase breaks the global $U(1)$ symmetry spontaneously. Then number of the domains N_D satisfies the scaling law

$$N_D \propto \tau_Q^{-d}, \quad (5)$$

where, τ_Q is the quench rate and exponent $d = 2\nu/(1 + \nu z)$. Here, ν is the critical exponent of the equilibrium correlation

length and z is the dynamical critical exponent. It is to be noted that these scaling laws are applicable at \hat{t} , which is the time at which the system transits from the impulse to the adiabatic domain. The details of locating \hat{t} are given in our previous work [43]. The same scaling law is also applicable to the defect density N_v . For the MI-SF transition the defects are the vortices and their density is given by [23–25, 43]

$$N_v = \sum_{p,q} |\Omega_{p,q}|, \quad (6)$$

with

$$\Omega_{p,q} = \frac{1}{4} [\sin(\theta_{p+1,q} - \theta_{p,q}) + \sin(\theta_{p+1,q+1} - \theta_{p+1,q}) - \sin(\theta_{p+1,q+1} - \theta_{p,q+1}) - \sin(\theta_{p,q+1} - \theta_{p,q})], \quad (7)$$

where, $\theta_{p,q}$ is the phase of $\phi_{p,q}$. In the results section we first calculate the critical exponent d from the defect density N_v . Then, we use our method to calculate N_D and show that we get similar value of the critical exponent based on N_D . This serves as an excellent cross checking of two different approaches to estimate the same critical exponent.

C. Results

To study the MI-SF non-equilibrium quench dynamics we consider system size of 100×100 . The Hamiltonian is scaled with U and time is defined in the units of \hbar/U . The hopping amplitude J is evolved using the following quench protocol,

$$J(t) = J_i + \frac{(J_c - J_i)}{\tau_Q}(t + \tau_Q). \quad (8)$$

With this protocol, we have, $J(-\tau_Q) = J_i$ and $J(0) = J_c$ is the QCP of the MI-SF phase transition. For our study we take $J_i = 0.0U$ and $J_f = 0.08U$, and fix the chemical potential $\mu = 0.41U$. The value of the μ is chosen so that it corresponds to the tip of the MI(1) lobe and $J_c = 0.042U$. Thus, at $t = -\tau_Q$, the system is in the MI(1) phase, and at $t = t_f$, it is in the SF phase when the quantum quench ends.

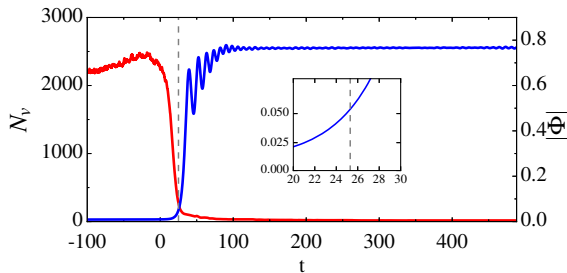


FIG. 8. The plot of the vortex density N_v as a function of time, shown in red color. And the plot of the $|\Phi|$ as a function of time is shown in blue color. The quantum critical point is crossed at $t = 0$, and the dashed grey line indicates the time instant \hat{t} .

1. Transition from MI to SF phase

As an indicator of the quench dynamics, the temporal evolution of $|\Phi| = \sum_{p,q} |\phi_{p,q}|/N_s$ and N_v during the quench, for $\tau_Q = 100$ are shown in Fig. 8. Here N_s denotes the number of lattice sites. In the initial stages of the quench dynamics, $|\Phi|$ is close to zero ($\sim 10^{-4}$), and remains so till \hat{t} . In the equilibrium MI state $|\Phi|$ is zero but in the quench dynamics it is finite due to the fluctuations added in the initial state preparation. As the QCP is crossed at $t = 0$, the system ought to evolve into SF phase ($t > 0$) and acquire a larger $|\Phi|$. But, as the system is still in the impulse domain, the $|\Phi|$ remains small till it ends at \hat{t} . Post \hat{t} , there is an exponential increase of $|\Phi|$, which is discernible from the plot in Fig. 8. After the exponential increase, the $|\Phi|$ settles to a steady state value.

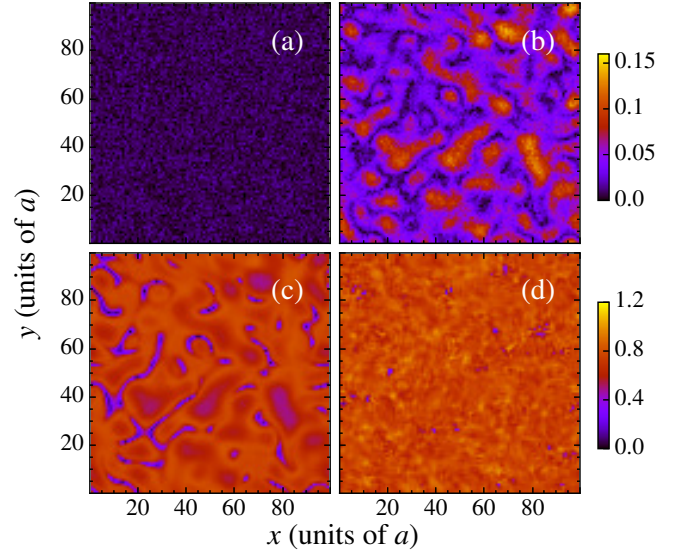


FIG. 9. Snapshots of $|\phi_{p,q}|$ at certain time instants for $\tau_Q = 100$. At initial times, $|\phi_{p,q}|$ is small, shown in (a). We see that its magnitude increases at $t = \hat{t}$, shown in (b). We note the domains of the SF order getting formed in the system, at $t = \hat{t}$. These domain structures disappear with the time, and the system gets homogeneous, as shown in (c) and (d).

The snapshots of $|\phi_{p,q}|$ at different times are shown in Fig. 9. The small values of $|\phi_{p,q}|$ at initial time $t = -\tau_Q$ is as shown in Fig. 9 (a). The figure also indicates the fluctuations present in the values of $|\phi_{p,q}|$. The Fig. 9 (b) shows the formation SF domains at \hat{t} when the system re-enter the adiabatic domain. The domains can be easily counted using our method. When J/U is further increased, these domains grow in size, and merge through the phase ordering process. This is visible from the Fig. 9 (c)-(d), in these figures $|\phi_{p,q}|$ is almost uniform.

The evolution of defect density N_v is complimentary to that of $|\Phi|$. At the initial stages of the quench, N_v is high (≈ 2200), this is due to the large phase fluctuations added to the initial state. It decrease after the system crosses QCP. This happens as the SF domains begin to form and phase coherence within the domains prevent the presence of a vortex

inside a domain. As time progresses, the phase ordering takes places, and these domains merge. The domain merger results in the annihilation of the vortex-antivortex pairs, further reducing N_v . This is discernible from the Fig. 8.

2. Critical exponents and scaling laws

To study the scaling of the N_v with τ_Q , we compute N_v over a range of τ_Q . As mentioned earlier, the scaling laws are considered at time \hat{t} . Hence, we compute N_v at \hat{t} for every τ_Q . The log-log plot of the values obtained are shown in Fig. 10 (a). From least square fitting, we get the value of the critical exponent d as 0.41. That is, $N_v \propto \tau_Q^{-0.41}$.

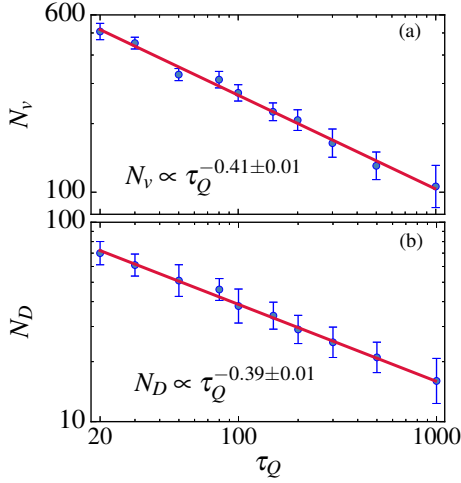


FIG. 10. Scaling of the vortex density N_v and number of domains N_D , with respect to τ_Q . From the plot (a), we see that the exponent $d = 0.41$. And from the plot (b), we notice that the scaling exponent, for the case of N_D versus τ_Q is 0.39. The blue error bars represent the standard deviation of the data values.

Following similar analysis, we determine the scaling exponent of the N_D with the quench rate. As shown in Fig. 9 (b), SF domains begins to appear at \hat{t} . These domains are characterized by a finite value of the SF order parameter. Since the MI regions also have a small non-zero SF order parameter, owing to the initial fluctuations, we set a threshold ϵ of the $|\phi_{p,q}|$ to distinguish the SF phase from the MI phase. The value of ϵ is taken as the average of $|\phi_{p,q}|$ over the prominent MI phase regions in the system at $t = 0$. In our computations, based on this definition, we get $\epsilon \approx 0.07$. We then calculate the ensemble-averaged value of N_D using our method. From the results, the scaling of N_D with τ_Q is as shown in Fig. 10 (b). We observe a power-law scaling is

$$N_D \propto \tau_Q^{-0.39}, \quad (9)$$

that is, the critical exponent $d = 0.39$. This implies that the scaling of the N_D with τ_Q is approximately same as the scaling of the N_v with τ_Q . This is expected from the KZM, as the density of the topological defects is used as a proxy for the number of domains. Thus, the domain counting algorithm

predicts an exponent that is in a good agreement with the exponent obtained from the vortex density. Here, it is to be noted that the methods used in computing N_D and N_v are different. One is based on the current distribution and our method is based on the identification of clusters. The two in essence serve as independent checks of the KZM scaling of the MI-SF transition.

VI. DISORDERED BOSE-HUBBARD MODEL

The analysis of the MI-SF quench dynamics utilized the domain counting aspect of the method we have developed. The fine-grained nature of the method also makes it suitable for detailed analysis of the clusters as well. We apply this to study the critical properties of the BG to SF transition in the 2D square optical lattice with disorder. The system is modeled with the disordered Bose-Hubbard model (DBHM). Earlier studies have identified the ground state phase diagram of the DBHM, and have shown the absence of a direct MI-to-SF transition [27–30, 46–48]. The MI-SF transition is intervened by the BG phase, which is characterized by non-zero compressibility and zero superfluid stiffness. Structurally, this is essentially MI phase inlaid with SF islands and the SF islands leads to the finite compressibility. However, the superfluid stiffness is zero as the islands cannot generate phase coherence across the system. Thus, in terms of percolation theory, the SF islands in the BG phase are non-percolating. But, the clusters percolate when the BG phase undergoes a transition to the SF phase. Therefore, the BG-to-SF transition can be viewed as the percolation analysis of the SF clusters. Previous works [49–51] have studied the geometric properties of the SF clusters, and compared the onset of superfluidity with the percolating transition of the system. In this work, we delve into the cluster properties using our method. In particular, we study the power-law divergence of the correlation length of the system near the percolating transition, and extract the critical exponent ν quantifying the divergence. The study reveals that the BG-to-SF transition falls in the percolation universality class of 2D lattice systems.

A. DBHM Hamiltonian

The DBHM Hamiltonian of the 2D square optical lattice is [27, 30, 49]

$$\hat{H} = - \sum_{\langle i,j \rangle} J \left(\hat{b}_i^\dagger \hat{b}_j + \text{H.c.} \right) + \sum_i \hat{n}_i \left[\frac{U}{2} (\hat{n}_i - 1) - \tilde{\mu}_i \right], \quad (10)$$

where, except for $\tilde{\mu}_i$ the model parameters have the same meaning as the BHM Hamiltonian in Eq.(2). Here, the effective chemical potential $\tilde{\mu}_i = \mu - \epsilon_i$ is site-dependent, and $\epsilon_i \in [-\Delta, \Delta]$ is a univariate random number to simulate diagonal disorder. The parameter Δ denotes the strength of the disorder. In the experiments, the disordered lattice potential is generated by shining a speckle beam [52–54].

The ground state phase diagram of the DBHM exhibits the quantum phases determined by the competition between the hopping energy J , the interaction energy U and the disorder strength Δ . For a moderate Δ , when J/U is small, the strong onsite repulsion favours the incompressible MI phase and atoms are pinned to the sites. For large J/U , the large hopping strength favours the compressible SF phase and atoms are itinerant. In the intermediate J/U the two phases are separated by the BG phase. As mentioned earlier, the BG is characterized by SF islands in the background sea of insulating MI phase. These islands impart finite number fluctuations $\delta n_{p,q}$ to the BG phase. Hence, $\delta n_{p,q}$ is an order parameter to distinguish the BG phase from the number coherent MI phase. For the site (p, q)

$$\delta n_{p,q} = \sqrt{\langle \hat{n}_{p,q}^2 \rangle - \langle \hat{n}_{p,q} \rangle^2}, \quad (11)$$

where the expectation value $\langle \dots \rangle$ is taken with respect to the ground state. At the BG-SF phase boundary, the SF stiffness ρ_s is the relevant order parameter to differentiate the BG and SF phases. It denotes the finite energy required to alter the phase of the wavefunction of the system. Since the SF phase is phase coherent, it exhibits a stiffness or resistance for the phase change. So, ρ_s is non-zero in the SF phase. But, it is zero in the MI and BG phases. To compute the ρ_s , we impose a twisted boundary condition along the x direction, transforming the hopping terms as [55]

$$J \left(\hat{b}_{p+1,q}^\dagger \hat{b}_{p,q} + \text{H.c.} \right) \rightarrow J \left(\hat{b}_{p+1,q}^\dagger \hat{b}_{p,q} e^{i2\pi\varphi/L_x} + \text{H.c.} \right),$$

where φ is the phase twist along the x direction hopping, and L_x is the system size along the x direction. The SF stiffness is then defined as

$$\rho_s = \frac{L}{8\pi^2} \frac{\partial^2 E_0}{\partial \varphi^2} \Big|_{\varphi=0}, \quad (12)$$

where E_0 is the ground state energy with twisted boundary condition.

For our studies on the statistics of the SF clusters in the BG phase, we choose the system size as 1000×1000 . The order parameters $\delta n_{p,q}$ and ρ_s are taken as ensemble average of 60 disorder realizations. Here, it is to be added that we observed finite-size effects for system sizes upto 200×200 that gave incorrect percolation transition point. The system size of 200×200 is, however, suitable for other studies like the determination of phase diagram, quench dynamics, etc.

B. Percolation analysis

The percolation theory analyses the statistical and geometrical properties of the clusters of sites on a lattice [4]. Specifically, in the site-percolation problem, every lattice site is independently and randomly *occupied* with probability p . The collection of neighbouring occupied sites is termed as a cluster. For small p , majority of the clusters constitute small number of sites, and are isolated. While for large p , majority of the

occupied sites form a percolating cluster which spans from one edge to the opposite edge. Thus, there exists a critical threshold probability p_c so that for $p < p_c$, there is no spanning cluster, and for $p \geq p_c$, there exists atleast one spanning cluster. Such a percolating transition is characterized by power-law divergences and universal critical exponents. One property which exhibits divergence at transition is the correlation length of the system ξ . It can be defined as an average over the cluster radii in the system

$$\xi^2 = \frac{\sum_s R_s^2 s^2 n_s}{\sum_s s^2 n_s}, \quad (13)$$

where R_s is the gyration radius of the cluster of s sites, and the n_s denotes the average number of clusters of size s per site. In the summation, the contribution from the infinite, percolating clusters is omitted [4, 5]. At the percolation transition ξ^2 shows power-law divergence

$$\xi^2 \propto |p - p_c|^{-\nu}.$$

The calculation of R_s involves the evaluation of the distance of a lattice site from the center of mass of the cluster [4, 5]. For systems with the periodic boundary conditions (PBC), due to the absence of edges, there are two possible definitions of the distance between two lattice sites. To resolve this in a consistent way, we unwrap the system. So that the clusters in the original system are mapped onto a system where dimensions are doubled. In the larger system, the distance between the lattice sites in a cluster are defined without ambiguity. The details of this procedure are given in the Appendix A.

In the BG phase, the sites with non-zero SF order parameter are considered as occupied sites. Hence, as the critical J_c of the BG-to-SF transition is approached, we expect the SF clusters to percolate. So, we can equivalently write the power law divergence in terms of reduced hopping strength as

$$\xi^2 \propto |J - J_c|^{-\nu}. \quad (14)$$

To identify the occupied sites we choose a threshold of 10^{-4} for the SF order parameter.

C. Results of BG-to-SF transition

For the percolation analysis we take $\Delta = 1.2U$ and $\mu = 0.2U$, and scan the phases as a function of J/U . The phase diagram in the $J/U - \mu/U$ plane, as reported in [30], constitutes the BG and SF phases. The absence of the MI phase is due to the high disorder strength. The snapshots of $|\phi_{p,q}|$ at different J/U are shown in Fig. 11 for a system of size 100×100 . As shown in Fig. 11 (a), the SF islands are isolated and the system is the BG phase. In Fig. 11 (b), the SF islands are larger but are non-percolating while in Fig. 11 (c) there exists percolating SF cluster and the system is in SF phase. And Fig. 11 (d) shows the profile of $|\phi_{p,q}|$ at large J/U .

In the Fig. 12 (a), the correlation length ξ^2 is shown as a function of J/U . As evident from the figure ξ^2 diverges at $J/U \approx 0.017$ and this signals a percolation transition from the

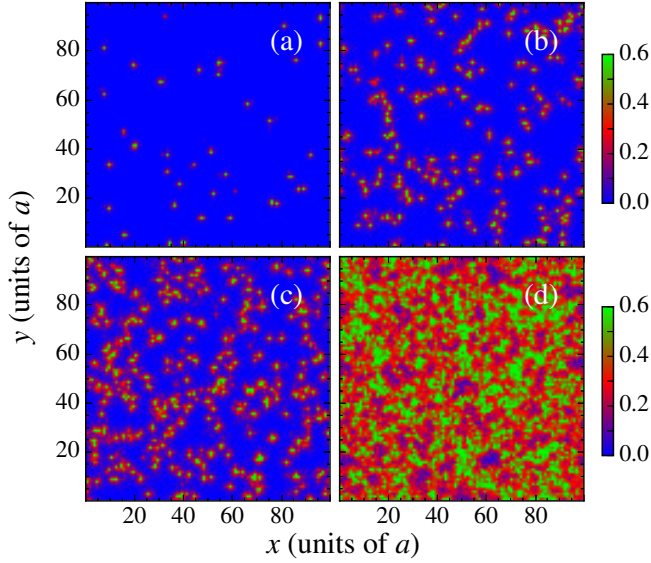


FIG. 11. Snapshots of $|\phi_{p,q}|$ at different J/U values. Panels (a)-(d) correspond to the J/U values as 0.009, 0.015, 0.019 and 0.025 respectively. As the J/U is increased, the SF domains percolate and the system undergoes a transition from BG to SF phase. Here $J_c \approx 0.017U$ for the system parameters $\mu = 0.2U$ and $\Delta = 1.2U$.

BG phase to the SF phase. Using the relation in Eq. (14) we can calculate the exponent ν which quantifies the divergence and obtain $\nu = 1.30 \pm 0.036$. This is in excellent agreement with the value of ν in the universality class of 2D random site percolation model. Previous studies [49, 56] have also computed the exponent ν and the values reported are in good agreement with our results. To study the BG-to-SF transition further, we plot ρ_s as a function of J/U in Fig. 12 (b). As mentioned earlier, ρ_s is small in the BG phase owing to the absence of a global phase coherence in the system. It shows an increase as the system enters the SF domain. Based on our previous work [30], we consider $\rho_s \approx 10^{-2}$ as a threshold for distinguishing between the BG and SF phase. The plot shows an increase in ρ_s at $J/U \approx 0.017$, and the threshold is crossed at $J = 0.0174U$. This is also the point where ξ^2 shows divergence. Thus, the identification of the BG-SF transition with the order parameter ρ_s matches with the percolation analysis. Given the fine-grained approach of our method, the properties of the domain formation and their dynamical evolution can be analysed using our method. This shall be addressed in our future works.

VII. CONCLUSION

To summarize, we have developed an algorithm to identify cluster or domain and study their percolation properties on a 2D lattice. The algorithm exploits the structure of the linked-lists data type, and enumerates the clusters on the lattice with a single scan. Further, the locations of the sites constituting a cluster are stored, and this facilitates the application of methods based on percolation theory. Our approach, with

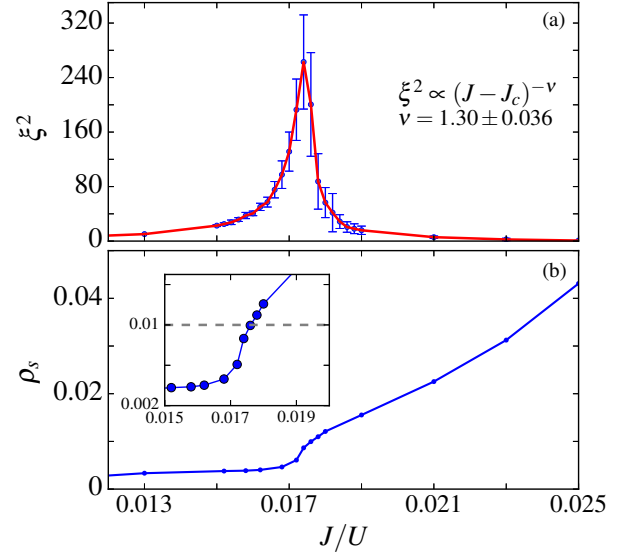


FIG. 12. Plot of the correlation length ξ and the superfluid stiffness ρ_s as a function of J/U . The chemical potential is $\mu = 0.2U$ and disorder strength is $\Delta = 1.2U$ for these calculations. The results are obtained by averaging over 60 disorder realizations. In plot (a), we observe a divergence of ξ , signaling the percolation transition from the BG to SF phase, with $J_c \approx 0.017U$. The critical exponent is $\nu = 1.30 \pm 0.036$. The standard deviation from the average value is shown by the blue error bar. Plot (b) denotes the stiffness ρ_s as a function of J/U . There is an noticeable increase in the stiffness near $J/U \approx 0.017$ as shown in the inset. For numerical calculations, the threshold value 0.01 (shown in gray dashed line) is considered to distinguish between the BG and SF phase.

minor modifications in the scanning process, can be adapted to lattices of higher dimensions. Based on the results, we also present an algorithm to identify the boundary of the cluster. Using the algorithm, we compute the number of domains formed in the MI-SF quench dynamics and calculate the critical exponent. The critical so obtained is in excellent agreement with the result from the vortex density. Further, we also studied the BG-SF transition in the DBHM. For this we calculate the correlation length of the SF clusters and observe a divergence near the BG-SF transition. The power-law exponent ν calculated suggests that the BG-SF transition belongs in the 2D lattice percolation universality class.

ACKNOWLEDGMENTS

The results presented in the paper are based on the computations using Vikram-100, the 100TFLOP HPC Cluster at Physical Research Laboratory, Ahmedabad, India. DA acknowledge the UGC SAP (DRS-II) project F.530/18/DRS-II/2018(SAP-I). The authors are grateful to Dr. S Pal, Dr. K Suthar, Dr. R Bai and Dr. S Bandyopadhyay for the critical reading and their comments to improve the manuscript.

Appendix A: System Unwrapping

We describe the unwrapping procedure employed on the system required to compute the distances within the system. The aim is to map the system of size $L_x \times L_y$ with periodic boundary conditions onto a larger system of size $2L_x \times 2L_y$ with open boundary condition. To begin with, we first identify the clusters on the boundary of the system. For illustration, consider a cluster that straddles across the left and right edge of the system. Due to the PBC, the left and right chunks are a part of same cluster. The chunk of this cluster connected with the right edge of the system needs a x-shift. The x-shift implies that the chunk is translated along the negative x direction by distance L_x . After this step, the two chunks ap-

pear side-by-side and the distance between any two points is unique. Similarly a y-shift is assigned to a chunk of the cluster which straddles along bottom and top edge. In some cases, a cluster may straddle across both directions. In this case, certain chunks may require both x-shift and y-shift. After these steps are performed, we compute the geometrical properties of the clusters. Here we mention that these steps are not valid for percolating clusters as they may be infinite in length, and would not accommodate in a new system of finite size. But as stated in the main text, the percolation analysis of the system generally ignores the contribution from the percolating clusters. And thus, the shifting of the finite sized non-percolating clusters suffices to perform the percolation studies.

-
- [1] S. R. Broadbent and J. M. Hammersley, "Percolation processes: I. crystals and mazes," *Mathematical Proceedings of the Cambridge Philosophical Society* **53**, 629–641 (1957).
 - [2] R. J. Elliott, B. R. Heap, D. J. Morgan, and G. S. Rushbrooke, "Equivalence of the critical concentrations in the ising and heisenberg models of ferromagnetism," *Phys. Rev. Lett.* **5**, 366–367 (1960).
 - [3] Paul J. Flory, *Principles of Polymer Chemistry* (Cornell University Press (New York), 1953).
 - [4] D. Stauffer and A. Aharony, *Introduction To Percolation Theory* (1992).
 - [5] Muhammad Sahimi and Allen G. Hunt, *Complex Media and Percolation Theory* (Springer, New York, NY, 2021).
 - [6] J. Hoshen and R. Kopelman, "Percolation and cluster distribution. i. cluster multiple labeling technique and critical concentration algorithm," *Phys. Rev. B* **14**, 3438 (1976).
 - [7] R.G. Moreira and M.A. Barrufet, "Spatial distribution of oil after deep-fat frying of tortilla chips from a stochastic model," *Journal of Food Engineering* **27**, 279–290 (1996).
 - [8] L. Zhang and N.A. Seaton, "Simulation of catalyst fouling at the particle and reactor levels," *Chemical Engineering Science* **51**, 3257–3272 (1996).
 - [9] M. Berry, J. Comiskey, and K. Minser, "Parallel analysis of clusters in landscape ecology," *IEEE Computational Science and Engineering* **1**, 24–38 (1994).
 - [10] F. Eddi, J. Mariani, and G. Waysand, "Transient synaptic redundancy in the developing cerebellum and isostatic random stacking of hard spheres," *Biological Cybernetics* **74**, 139–146 (1996).
 - [11] J. Hoshen, M. W. Berry, and K. S. Minser, "Percolation and cluster structure parameters: The enhanced hoshen-kopelman algorithm," *Phys. Rev. E* **56**, 1455–1460 (1997).
 - [12] S. Frijters, T. KrÄ¼ger, and J. Harting, "Parallelised hoshen-kopelman algorithm for lattice-boltzmann simulations," *Computer Physics Communications* **189**, 92–98 (2015).
 - [13] Jeffrey M. Constantin, Michael W. Berry, and Bradley T. Vander Zanden, "Parallelization of the hoshen-kopelman algorithm using a finite state machine," *The International Journal of Supercomputer Applications and High Performance Computing* **11**, 34–48 (1997).
 - [14] Nicholas R. Moloney and Gunnar Pruessner, "Asynchronously parallelized percolation on distributed machines," *Phys. Rev. E* **67**, 037701 (2003).
 - [15] J.M. Teuler and J.C. Gimel, "A direct parallel implementation of the hoshen-kopelman algorithm for distributed memory architectures," *Computer Physics Communications* **130**, 118–129 (2000).
 - [16] Norbert Sendra, Tomasz GwizdaÅa, and Jerzy Czerbniak, "Reducing algorithm for percolation cluster analysis," *Annales Universitatis Mariae Curie-Sklodowska, sectio AI-Informatica* **5**, 87–91 (2006).
 - [17] M. E. J. Newman and R. M. Ziff, "Efficient monte carlo algorithm and high-precision results for percolation," *Phys. Rev. Lett.* **85**, 4104–4107 (2000).
 - [18] T W B Kibble, "Topology of cosmic domains and strings," *Journal of Physics A: Mathematical and General* **9**, 1387 (1976).
 - [19] T.W.B. Kibble, "Some implications of a cosmological phase transition," *Physics Reports* **67**, 183 (1980).
 - [20] W. H. Zurek, "Cosmological experiments in superfluid helium?" *Nature* **317**, 505 (1985).
 - [21] W.H. Zurek, "Cosmological experiments in condensed matter systems," *Physics Reports* **276**, 177 (1996).
 - [22] Adolfo del Campo and Wojciech H. Zurek, "Universality of phase transition dynamics: Topological defects from symmetry breaking," *International Journal of Modern Physics A* **29**, 1430018 (2014).
 - [23] Keita Shimizu, Yoshihito Kuno, Takahiro Hirano, and Ikuo Ichinose, "Dynamics of a quantum phase transition in the bose-hubbard model: Kibble-zurek mechanism and beyond," *Phys. Rev. A* **97**, 033626 (2018).
 - [24] Keita Shimizu, Takahiro Hirano, Jonghoon Park, Yoshihito Kuno, and Ikuo Ichinose, "Out-of-equilibrium dynamics of multiple second-order quantum phase transitions in an extended bose-hubbard model: Superfluid, supersolid, and density wave," *Phys. Rev. A* **98**, 063603 (2018).
 - [25] Keita Shimizu, Takahiro Hirano, Jonghoon Park, Yoshihito Kuno, and Ikuo Ichinose, "Dynamics of first-order quantum phase transitions in extended bose-hubbard model: from density wave to superfluid and vice versa," *New Journal of Physics* **20**, 083006 (2018).
 - [26] Yijia Zhou, Yongqiang Li, Rejish Nath, and Weibin Li, "Quench dynamics of rydberg-dressed bosons on two-dimensional square lattices," *Phys. Rev. A* **101**, 013427 (2020).
 - [27] M. P. A. Fisher, P. B. Weichman, G. Grinstein, and D. S. Fisher, "Boson localization and the superfluid-insulator transition," *Phys. Rev. B* **40**, 546 (1989).

- [28] P. Buonsante, V. Penna, A. Vezzani, and P. B. Blakie, “Mean-field phase diagram of cold lattice bosons in disordered potentials,” *Phys. Rev. A* **76**, 011602 (2007).
- [29] L. Pollet, N. V. Prokof’ev, B. V. Svistunov, and M. Troyer, “Absence of a direct superfluid to mott insulator transition in disordered bose systems,” *Phys. Rev. Lett.* **103**, 140402 (2009).
- [30] S. Pal, R. Bai, S. Bandyopadhyay, K. Suthar, and D. Angom, “Enhancement of the bose glass phase in the presence of an artificial gauge field,” *Phys. Rev. A* **99**, 053610 (2019).
- [31] A. Newell and J. C. Shaw, “Programming the logic theory machine,” in *Proceedings of the Western Joint Computer Conference* (Association for Computing Machinery (New York), 1957).
- [32] D. Jaksch, C. Bruder, J. I. Cirac, C. W. Gardiner, and P. Zoller, “Cold bosonic atoms in optical lattices,” *Phys. Rev. Lett.* **81**, 3108 (1998).
- [33] Simon Braun, Mathis Friesdorf, Sean S. Hodgman, Michael Schreiber, Jens Philipp Ronzheimer, Arnau Riera, Marco del Rey, Immanuel Bloch, Jens Eisert, and Ulrich Schneider, “Emergence of coherence and the dynamics of quantum phase transitions,” *Proceedings of the National Academy of Sciences* **112**, 3641 (2015).
- [34] M. Greiner, O. Mandel, T. Esslinger, T. W. Hänsch, and I. Bloch, “Quantum phase transition from a superfluid to a Mott insulator in a gas of ultracold atoms,” *Nature (London)* **415**, 39 (2002).
- [35] Markus Greiner, Olaf Mandel, Theodor W. Hänsch, and Immanuel Bloch, “Collapse and revival of the matter wave field of a bose-einstein condensate,” *Nature* **419**, 51 (2002).
- [36] D. S. Rokhsar and B. G. Kotliar, “Gutzwiller projection for bosons,” *Phys. Rev. B* **44**, 10328 (1991).
- [37] K. Sheshadri, H. R. Krishnamurthy, R. Pandit, and T. V. Ramakrishnan, “Superfluid and insulating phases in an interacting-boson model: Mean-field theory and the RPA,” *EPL* **22**, 257 (1993).
- [38] R. Bai, S. Bandyopadhyay, S. Pal, K. Suthar, and D. Angom, “Bosonic quantum Hall states in single-layer two-dimensional optical lattices,” *Phys. Rev. A* **98**, 023606 (2018).
- [39] Soumik Bandyopadhyay, Rukmani Bai, Sukla Pal, K. Suthar, Rejish Nath, and D. Angom, “Quantum phases of canted dipolar bosons in a two-dimensional square optical lattice,” *Phys. Rev. A* **100**, 053623 (2019).
- [40] K. Suthar, Hrushikesh Sable, Rukmani Bai, Soumik Bandyopadhyay, Sukla Pal, and D. Angom, “Supersolid phase of the extended bose-hubbard model with an artificial gauge field,” *Phys. Rev. A* **102**, 013320 (2020).
- [41] Rukmani Bai, Deepak Gaur, Hrushikesh Sable, Soumik Bandyopadhyay, K. Suthar, and D. Angom, “Segregated quantum phases of dipolar bosonic mixtures in two-dimensional optical lattices,” *Phys. Rev. A* **102**, 043309 (2020).
- [42] Kuldeep Suthar, Rebecca Kraus, Hrushikesh Sable, Dilip Angom, Giovanna Morigi, and Jakub Zakrzewski, “Staggered superfluid phases of dipolar bosons in two-dimensional square lattices,” *Phys. Rev. B* **102**, 214503 (2020).
- [43] Hrushikesh Sable, Deepak Gaur, Soumik Bandyopadhyay, Rejish Nath, and D. Angom, “Quantum quench dynamics of tilted dipolar bosons in 2d optical lattices,” (2021), [arXiv:2106.01725](https://arxiv.org/abs/2106.01725).
- [44] Bogdan Damski, “The simplest quantum model supporting the kibble-zurek mechanism of topological defect production: Landau-zener transitions from a new perspective,” *Phys. Rev. Lett.* **95**, 035701 (2005).
- [45] Bogdan Damski and Wojciech H. Zurek, “Adiabatic-impulse approximation for avoided level crossings: From phase-transition dynamics to landau-zener evolutions and back again,” *Phys. Rev. A* **73**, 063405 (2006).
- [46] Ulf Bissbort, Ronny Thomale, and Walter Hofstetter, “Stochastic mean-field theory: Method and application to the disordered bose-hubbard model at finite temperature and speckle disorder,” *Phys. Rev. A* **81**, 063643 (2010).
- [47] P. Pisarski, R. M. Jones, and R. J. Gooding, “Application of a multisite mean-field theory to the disordered bose-hubbard model,” *Phys. Rev. A* **83**, 053608 (2011).
- [48] Ş. G. Söyler, M. Kiselev, N. V. Prokof’ev, and B. V. Svistunov, “Phase diagram of the commensurate two-dimensional disordered bose-hubbard model,” *Phys. Rev. Lett.* **107**, 185301 (2011).
- [49] A E Niederle and H Rieger, “Superfluid clusters, percolation and phase transitions in the disordered, two-dimensional bose-hubbard model,” *New Journal of Physics* **15**, 075029 (2013).
- [50] Sk Noor Nabi and Saurabh Basu, “Percolation analysis of a disordered spinor bose gas,” *Journal of Physics B: Atomic, Molecular and Optical Physics* **49**, 125301 (2016).
- [51] Apurba Barman, Sunayana Dutta, Ayan Khan, and Saurabh Basu, “Understanding the bose glass phase via a percolation scenario,” *The European Physical Journal B* **86**, 308 (2013).
- [52] D. Clément, A. F. Varón, M. Hugbart, J. A. Retter, P. Bouyer, L. Sanchez-Palencia, D. M. Gangardt, G. V. Shlyapnikov, and A. Aspect, “Suppression of transport of an interacting elongated bose-einstein condensate in a random potential,” *Phys. Rev. Lett.* **95**, 170409 (2005).
- [53] D. Clément, P. Bouyer, A. Aspect, and L. Sanchez-Palencia, “Density modulations in an elongated bose-einstein condensate released from a disordered potential,” *Phys. Rev. A* **77**, 033631 (2008).
- [54] M. White, M. Pasienski, D. McKay, S. Q. Zhou, D. Ceperley, and B. DeMarco, “Strongly interacting bosons in a disordered optical lattice,” *Phys. Rev. Lett.* **102**, 055301 (2009).
- [55] M Gerster, M Rizzi, F Tschirsich, P Silvi, R Fazio, and S Montangero, “Superfluid density and quasi-long-range order in the one-dimensional disordered bose-hubbard model,” *New Journal of Physics* **18**, 015015 (2016).
- [56] Juan Pablo Álvarez Zúñiga, David J. Luitz, Gabriel Lemarié, and Nicolas Laflorencie, “Critical properties of the superfluid—bose-glass transition in two dimensions,” *Phys. Rev. Lett.* **114**, 155301 (2015).